

Experimental measurement of heat transfer coefficient in two phase flow of binary zeotropic mixture in a horizontal tube

Michal Haubner^{1*}, David Houška¹, Martin Doubek¹, Václav Vacek^{1,2}

¹ Department of Physics, Faculty of Mechanical Engineering, Czech Technical University in Prague, Czech Republic
² supervisor

Abstract

The heat transfer coefficient of boiling in a horizontal tube was measured for a binary zeotropic mixture of perfluorocarbons. The investigated mixture composition varied from 5% to 25% C₂F₆ in C₃F₈, with the step of 5%. The paper describes the process of construction and commissioning of the measurement setup, then outlines a measurement procedure and finally the acquired data is analysed and discussed. Data acquisition system based on SIEMENS WinCC software was used for monitoring, visualisation and archiving of the measured data, whereas further data processing was performed in MATLAB environment. Thorough data analysis revealed multiple flow regimes of the two phase flow that varied as a function of coolant flow rate, heat flux, vapour quality and mixture composition. Moreover, this experiment is an accurate model of the ATLAS SCT inner detector cooling circuit and it has a potential of direct application during the planned upgrade of the detector's cooling system.

Key words: Boiling in a horizontal tube, two phase flow, flow regime, data acquisition, measurement of heat transfer coefficient, ATLAS SCT inner detector cooling.

1 Heat transfer coefficient

1.1 Introduction

The heat transfer coefficient (HTC) h [W/m².K] relates the heat flux \dot{Q} [W] through a fluid-wall interface to the temperature difference ΔT [K] between the wall and the fluid. The seemingly simple Newton's law of convective heat transfer (Figure 1) gives rise the HTC, which itself contains all nonlinearities, whereas the rest of the equation remains nicely linear. As outlined in [1], the heat transfer can occur under a wide range of conditions, the HTC value also spans over 5 magnitudes, depending on the fluid concerned, character of convection (natural, forced, boiling, etc.), and the surface geometry (wall, tube, etc.).

$$\dot{q} = h \cdot \Delta T \quad (1)$$

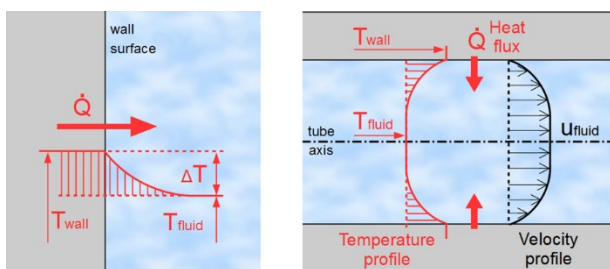


Figure 1. Basic cases of heat transfer.

For high power density applications (e.g. cooling of electronics) it is desirable to have efficient cooling systems, which are capable of dissipating high heat fluxes through a relatively small area. As can be derived from the basic heat transfer formula, the heat flux \dot{q} can be increased either by increasing ΔT , which is not always possible, or by increasing the HTC, which is usually the case. The highest HTC values are achieved during a phase change. This fact immediately places the process of boiling and condensation of a refrigerant into an engineering interest.

Motivation for the presented study arises from the cooling circuit of ATLAS inner detector, called Semiconductor tracker (SCT), which is described in detail in [2]. Efficient cooling is necessary not only to dissipate the heat generated in a very confined space formed by the detector barrels. It keeps the temperatures low enough for a good signal-to-noise ratio of the readout electronics and also slows down aging caused by radiation. Current SCT detector cooling does not perform as well as it was designed to and moreover the detector life-time is about to be prolonged. As published in [3] it is of consideration to add a small amount of C₂F₆ to currently pure C₃F₈ refrigerant in order to gradually decrease temperatures in the system by lowering the saturation temperature of the refrigerant blend.

1.2 Heat transfer with phase change

This study investigates evaporation of a binary refrigerant mixture in a tube heat exchanger, which is designed to cool down electronics mounted on its outer surface. Boiling in a horizontal tube occurs in several different flow patterns, depending on a vapour quality, flow velocity and heat flux. As described by Collier in [4] and as can be seen in a graphics of his in Figure 2, these parameters may change with position along the tube, thus changes the local value of HTC, which is strongly bounded to the local flow pattern.

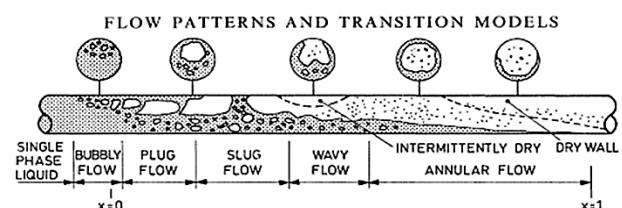


Figure 2. Flow patterns during boiling in a horizontal tube. As published by Collier John G. in [4].

* Corresponding author: Michal.Haubner@fs.cvut.cz

1.3 Zeotropic mixture evaporation process

The p-h diagram for 20% C₂F₆ in C₃F₈ mixture shows that the evaporation process is not isobaric isothermal change, as it is in the case of a pure compound. In fact, the temperatures of saturated liquid and saturated vapour differ. An idealized process of throttling (capillary) and heating (stave) is depicted in the Figure 3.

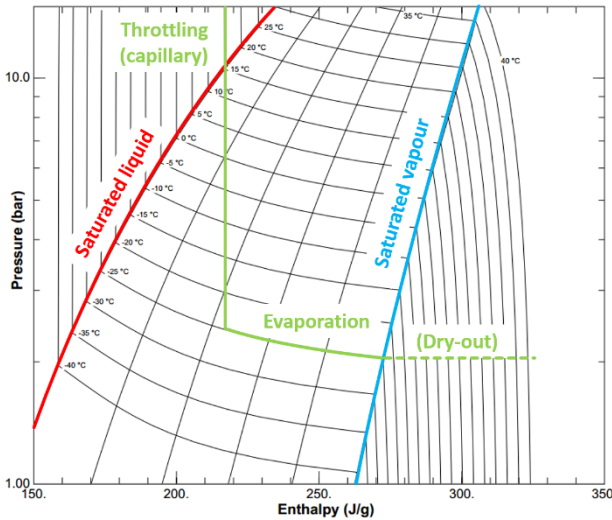


Figure 3. Idealized processes described in p-h diagram for 20% C₂F₆ mixture, generated by NIST REFPROP [5].

2 Construction of the experiment

2.1 Experimental stand

Since this research is motivated by the cooling of electronics inside a particle detector, it was decided to use the exact same tube heat exchanger as in real application: 0.2 mm thin wall copper-nickel tube with 4 mm inner diameter, called 'stave'. To simulate the heat load and to account for the convective heat transfer only, it was decided to use Joule heating, as it generates a uniform heat load distribution along the stave in a precisely defined geometry.

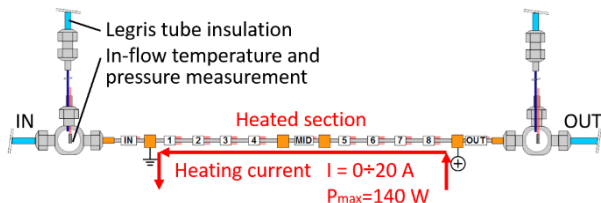


Figure 4. Pressure tapping and temperature read-out mounted in a Swagelok T-fitting for direct in-flow measurement.

2.2 Temperature sensors

The whole stave was equipped with a number of temperature sensors, allowing for precise information about temperature profile, temperature gradients and also providing information about the evaporation process inside the stave. The Pt1000 sensors were used exclusively, due to their accuracy. Sensors were mounted

both on the top and the bottom of the stave, as stratified flow regimes were expected under certain conditions. The sensors placement and the method of their fixation on the tube surface are introduced in Figure 5. The sensors were calibrated inside the anticipated temperature range from -30°C to 30°C, prior to their installation.

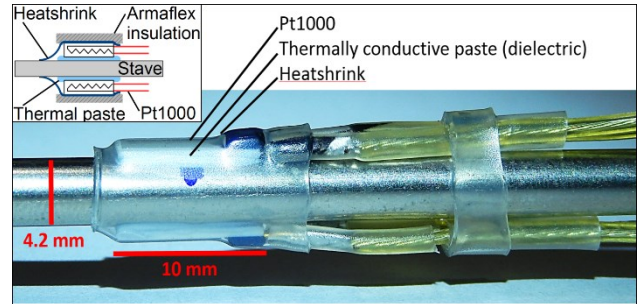


Figure 5. Pt1000 mounted on top and bottom sides of the stave. Proper thermal interface is ensured by dielectric thermal paste.

2.3 Pressure sensors

A Keller high-precision absolute pressure sensor was used to measure the saturation pressure at the stave inlet, whereas a HUBA differential pressure sensor measured pressure drop along the stave.

Temperature and pressure at the inlet and outlet of the stave was measured directly in the flow using sensors mounted in Tee-fittings, as seen in Figure 6. The precise knowledge of saturation temperature and pressure is crucial for the calculation of vapour quality and hence the enthalpy entering and leaving the system (stave).

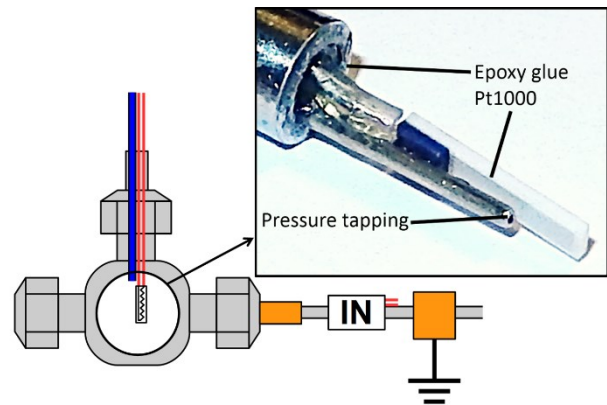


Figure 6. Pressure tapping and temperature read-out mounted in a Swagelok T-fitting for direct in-flow measurement.

2.4 Power terminals

The use of Joule principle for heating requires a system of power terminals, grounding, insulation and sense wires. The stave itself is resting on an Armaflex foam and is connected by Legris tubing, which forms insulation from the support. A set of copper power terminals is soldered to the stave to form a circuit for heating and to define a precise length of the heated section. The heated section is 82cm long, whereas the rest of the tube was used for soldering the inlet and outlet

manifold. The copper blocks are equipped with sense wires, which are directly connected to the ELMB DAQ system in order to measure the actual voltage drop along the stave excluding the influence of power supply cables. Finally, the dissipated power is derived from the measured potential difference and known resistance of the heated section.

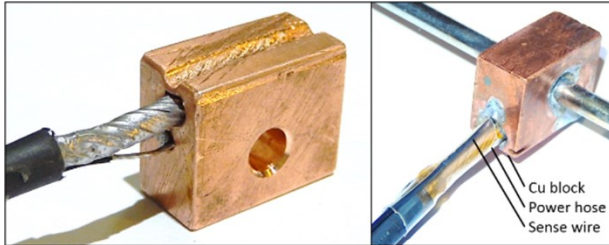


Figure 7. Power terminal connection to stave. Note the connection of power hose and sense-wire.

2.5 Technical support

A closed loop cooling plant was necessary to operate the setup. The cooling circuit supplies liquid refrigerant at 14 bara and room temperature and pumps back refrigerant vapour at 1.2 bara. The refrigerant mass flow through the stave was set by a pair of capillaries and stabilised by a pressure and back-pressure regulators. The temperature of liquid refrigerant at the input of capillaries was maintained at temperature of 15 ± 1 °C by a glycol-circulating chiller coupled with counter-flow heat exchanger. Extra 30 meters of tubing is present to simulate the inertia of the real cooling loop.

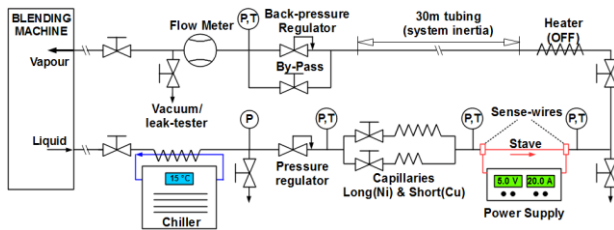


Figure 8. Coolant recirculation machine, technical support and instrumentation for the stave measurement setup.

3 Data acquisition and visualisation

Given the number of various sensors and the nature of phenomenon observed, a sophisticated DAQ system is needed. A combination of Embedded Local Monitoring Board (ELMB) and open architecture SIEMENS WinCC software was used, as it integrates all necessary features of SCADA system. All components of the DAQ chain have been separately calibrated prior to their installation in the experiment in order to obtain as precise reading as possible. Both inner and outer calibration was performed on the ELMB as well to ensure its accuracy.

3.1 ELMB calibration

The ELMB was calibrated in two steps: inner and outer calibration. During the inner calibration all adapters were

dismounted, their resistance was measured and it was found that their nominal resistance varies by about $\pm 1\%$. The outer calibration was also performed by connecting all ELMB channels to a set of high precision resistors of various nominal resistances to obtain the ELMB reading over the range of the temperature sensors resistances. Finally both corrections were taken into account and directly embedded in the PVSS software to be used during the forthcoming measurements.



Figure 9. ELMB Motherboard (rear side) with mounted ELMB unit and equipped with voltage and resistance adapters.

3.2 Graphical user interface

A simple graphical user interface (GUI) was developed in the PVSS environment to observe all system parameters in real time. It greatly simplified the commissioning and measurement process, as the user can easily take a precise control of various parameters of the experiment.

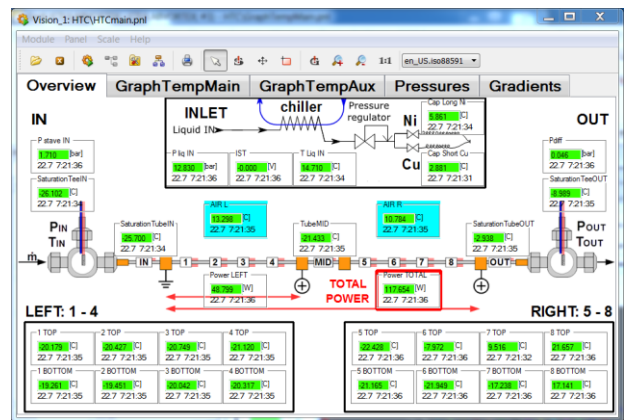


Figure 10. User Graphical user interface visualizing all important values of pressure, temperature and power.

4 Measurements

4.1 Measured dataset

The similar dataset was acquired for each mixture composition, i.e. from 5 to 25 % of C_2F_6 in C_3F_8 (by molar fraction) with a step of 5%. Higher concentrations were not possible to achieve with the setup, as the saturation pressure drops below 13 bara for a mixture 30% C_2F_6 . The range of pressures and flow-rates shown in Table 1 was carefully chosen in order to simulate the real detector cooling circuit conditions. The upper part of the table represents uniform heating along the whole stave, whereas the bottom part represents the case when only

the first half of stave is heated and its down-stream influence is investigated.

Table 1. Dataset measured for each refrigerant composition.

P_{IN} [bara]	P_{OUT} [bara]	Flow rate [g/s]	Stave Heating [W]					
13	1.5	2	0	37	52	81	104	122
	2.5		0	37	52	81	104	122
13	1.5	1.5	0	37	52	81	104	122
	2.5		0	37	52	81	104	122
13	1.5	3.5	0	37	52	81	104	122
	2.5		0	37	52	81	104	122
P_{IN} [bara]	P_{OUT} [bara]	Flow rate [g/s]	Only 1 st Half of Stave Heated [W]					
13	1.5	0	15	33	58			
	2	2	15	33	58			
	2.5	0	15	33	58			

4.2 Preparing a mixture

Once the full dataset for investigated refrigerant composition was collected and a preliminary data analysis with coherent results were registered, more C_2F_6 was added to the cooling plant in order to increase the C_2F_6 fraction in the mixture. The procedure was done by adding a precise amount of C_2F_6 from gas cylinder to the blending machine's condenser. Then the refrigerant mixture present in the system was properly homogenized by letting the system run at full power mode for several hours. The composition was precisely verified by sonar tube gas analyser (Figure 11) at the end of the mixing process. The sonar gas analyser is an integral part of the blending machine and the instrument was developed earlier at the Department of Physics of the Mechanical Engineering faculty at the CTU in Prague. This development is thoroughly described in [6 -8].

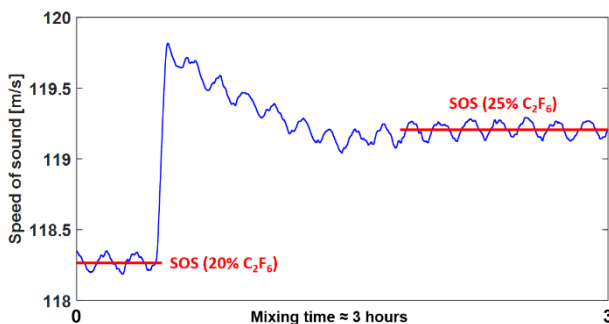


Figure 11. Speed of sound measurement for refrigerant composition verification performed during mixing procedure.

4.3 Premeasurement calibration

The dataset in Table 1 was measured line by line. Every measurement began with a stabilization of the system without heating and consequent 10 minute reading of the stable system. This reading served as a baseline, or a premeasurement calibration of the temperature

sensors, also called zeroing. Once the zeroing was done, different heating powers were applied one by one in an increasing manner to avoid possible overheating.

Measured values were averaged over 10 minute long interval and plotted with respect to position on the stave. Presumably, the most precise reading of saturation temperature comes from in-flow sensors mounted in Tee-fittings. However, the two temperatures measured in the input and output Tee-fittings were not the same due to the pressure difference over the stave and the temperature glide of the zeotropic blends. Linear interpolation was used (black line in Figure 12) to obtain a representation of saturation temperature along the whole length of the stave. The linear relation is not entirely valid for the blends, but it is sufficiently accurate for the first analysis.

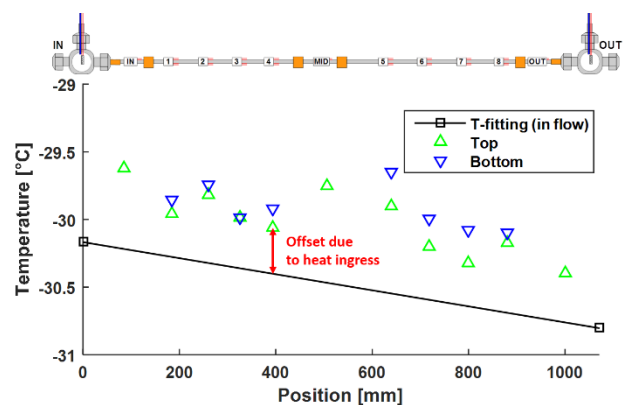


Figure 12. Heat ingress results in offset of temperature reading.

Taking the interpolation of the saturation temperatures measured in the flow (black line) as a baseline, one can see that all sensors mounted on the stave surface read slightly higher values than expected. This difference results mainly from the temperature gradient between the stave surface ($-30\text{ }^{\circ}\text{C}$) and ambient air ($10\text{ }^{\circ}\text{C}$). Moreover, the sensors probably show a scatter as a result from non-uniform thermal contact, even though all sensors were mounted using the very same technology.

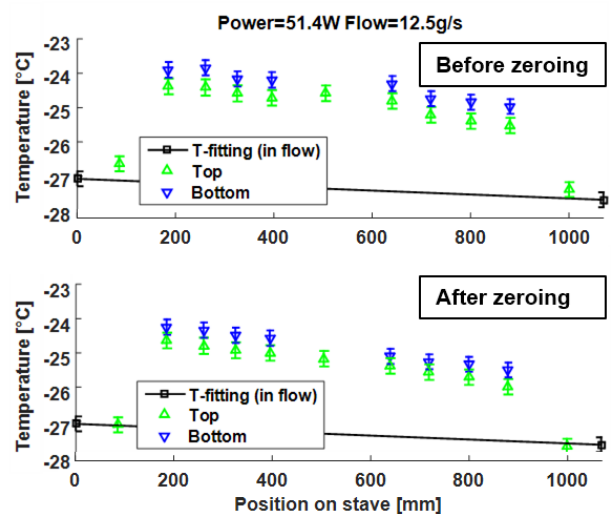


Figure 13. Effect of premeasurement calibration (zeroing) on a processed data sample.

5 Data analysis

According to Newton's cooling law, the HTC is calculated as a ratio of the heat flux \dot{q} and temperature difference ΔT . The heat flux through the stove surface is given by the ratio of dissipated Joule heat and the stove heated section inner surface. The temperature difference is determined as a difference between the wall temperature and the temperature of fluid far from the wall (beyond the thermal boundary layer). The fluid temperature was linearly interpolated between the two in-flow temperature readings. Lastly, the heat flux was determined from the dissipated Joule heat and the inner surface of the (82 cm).

$$h = \frac{\dot{q}}{\Delta T} \quad (2)$$

5.1 Data processing in MATLAB

The sophisticated DAQ system provided a massive amount of data, which had to be evaluated. The MATLAB environment was ideal for this task, as it easily processes extensive datasets. Measured data were exported from PVSS software in a .csv format, which was loaded into the MATLAB and processed with a series of developed programs. NIST REFPROP database [2] was used to determine the thermodynamic properties and to calculate enthalpy and vapour quality throughout the system. For a sample of processed data, see Figure 14.

5.2 Flow regimes

Different flow regimes were observed as a function of flow rate and heat flux. Such phenomenon is visible

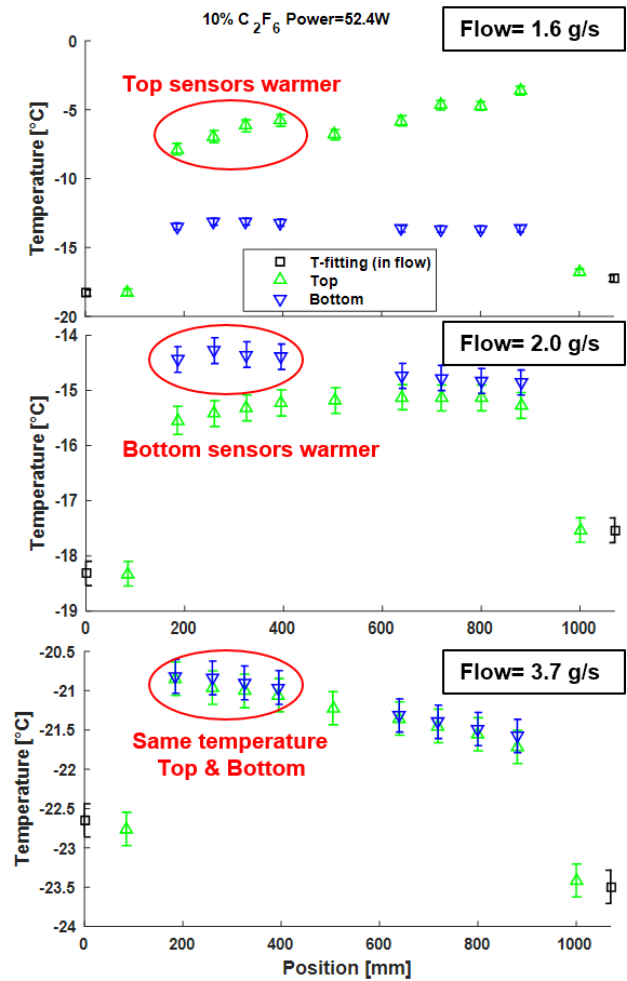


Figure 15. Flow regimes vs. flow rate during one measurement.

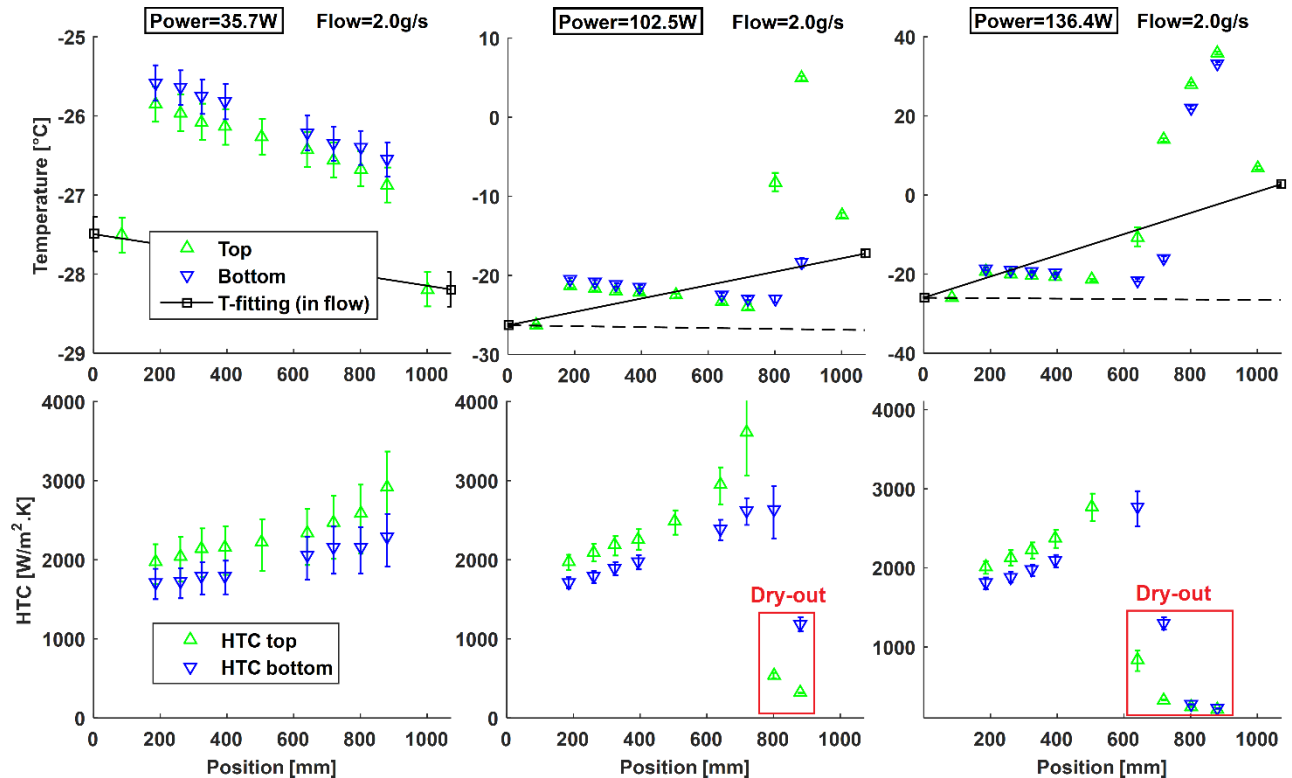


Figure 14. Sample measurement for 5% C₂F₆ and flow rate of 2 g/s. This data sample shows one moderate heat flux and two high heat fluxes with dry-out conditions.

in the Figure 15 and can be well compared to some basic cases depicted in the Figure 2, originally published by Collier and Thome in [4].

The composition and power were kept constant in this figure, whereas the flow rates varied from 1.6 to 3.7 g/s. The bottom side of the stove showed lower temperatures and consequently greater HTC at the flow rate of 1.6 g/s. This phenomenon alternated at 2 g/s and the difference completely vanished at high flow of 3.7 g/s. These results suggest, that the “concentric annular” flow regime was obtained for flow rates higher than 3 g/s, where the turbulence is already high enough to counter the effect of gravity.

A rare case of higher HTC on the top of the stove was observed for the flow rate of 2 g/s. Its origin as well as precise conditions remained unclear and it will have to be investigated further on.

5.3 Dry-out

So called “dry out” condition is a regime, when the most of the liquid refrigerant has evaporated, no liquid is in contact with the pipe wall and consequently the HTC drops considerably and tube temperature rises. In other words, when all latent heat is used, the evaporation of a liquid is replaced by forced convection of vapour, which is not nearly as efficient in transferring heat. The vapour then superheats and the stove outlet temperature rises significantly.

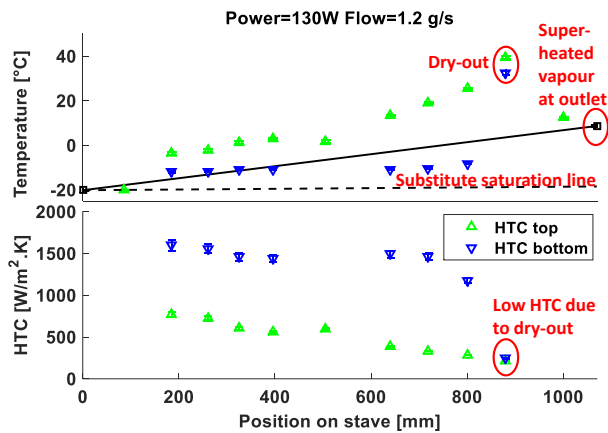


Figure 16. Dry-out occurrence on the last pair of sensors.

5.4 Partial dry-out

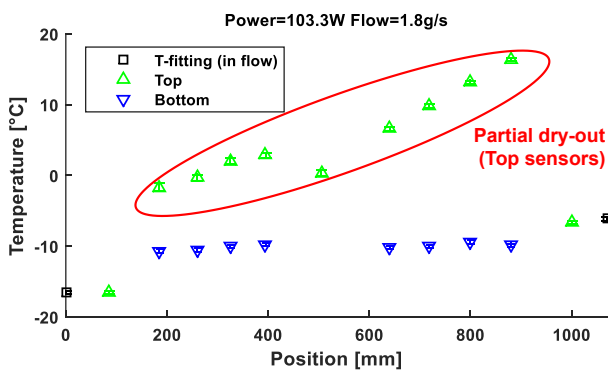


Figure 17. Partial dry out on the top sensors.

A partial dry-out is a case of flow stratification, which was observed at low refrigerant flow rates. The lower the flow rate the lower the turbulence and the more the fluid tends to pool at the bottom of the tube, which results into higher HTC at the bottom of the stove, as it can be seen in the Figure 17.

5.5 HTC vs. evaporation pressure

Figure 18 shows the severely negative influence of evaporation pressure on the HTC. Apart from that, note the smooth and equalized dependence of HTC on vapour quality for higher evaporation pressure.

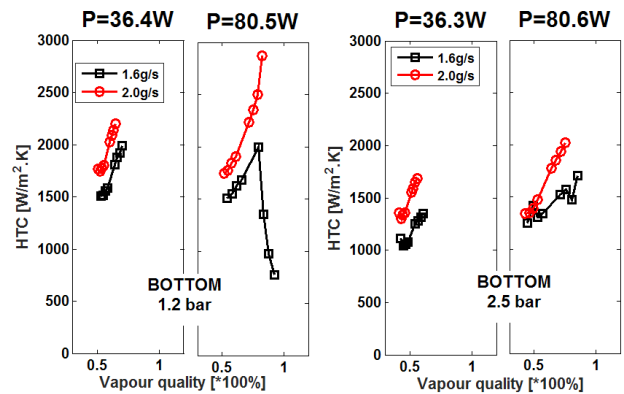


Figure 18. Change of HTC with evaporation pressure.

5.6 Thermal boundary layer evolution

A series of measurement with only partial heating on the first half of the stove was conducted to observe the thermal boundary layer development and its effect downstream. Such measurement is showed below in Figure 19. Despite the high heat flux, total dry-out was not reached. The tube temperature returned to the saturation temperature within 10cm after the heated section.

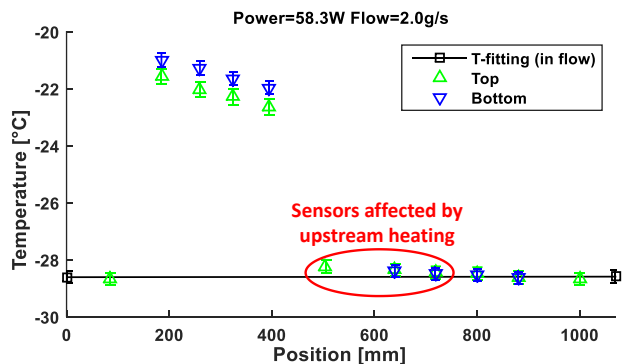


Figure 19. Boundary layer evolution during half heating.

5.7 Mass flow vs. composition

It was observed during the measurements, that the mass flow dropped slightly after each mixing procedure. This effect was assigned to the change of density and viscosity of the fluid, which resulted into different flow-rates on the same pressure difference. The pressure drop was

maintained constant for all mixture compositions, because in the real detector's cooling circuit, multiple pressure and back-pressure regulators are used to stabilize the system.

Table 2. Mass-flow change with concentration at constant pressure difference.

Capillary C ₂ F ₆ fraction	1 [g/s]	2 [g/s]	1+2 [g/s]
5%	1.71	2.02	3.79
10%	1.59	1.96	3.62
15%	1.45	1.73	3.31
20%	1.42	1.75	3.20
25%	1.35	1.63	3.11

5.8 Temperature vs. composition

A dependence of maximum stave temperature on mixture composition was observed as a result of the HTC measurements for different blends. Note that this plot represents high mass flows, so that dry out conditions are

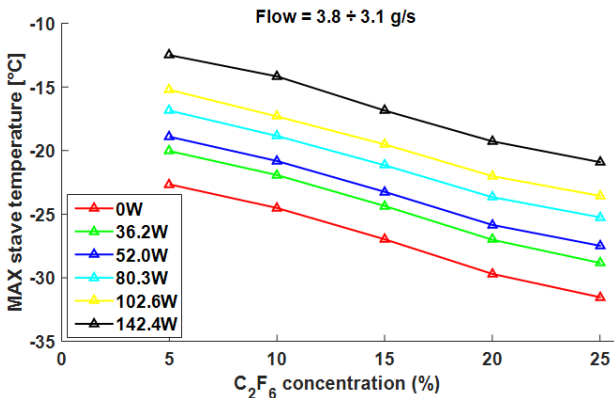


Figure 20. Maximum stave temperature vs. composition.

avoided in all cases. The gradual decrease of temperature is observed with increasing C₂F₆ concentration, because the saturation temperature gradually drops as well. This dependence is evident for all heat fluxes and even for the highest heat flux of 142 W.

5.9 HTC vs. composition

The HTC dependency on concentration has been also evaluated. It can be concluded from Figure 21, that HTC gradually decreases with increasing C₂F₆ fraction

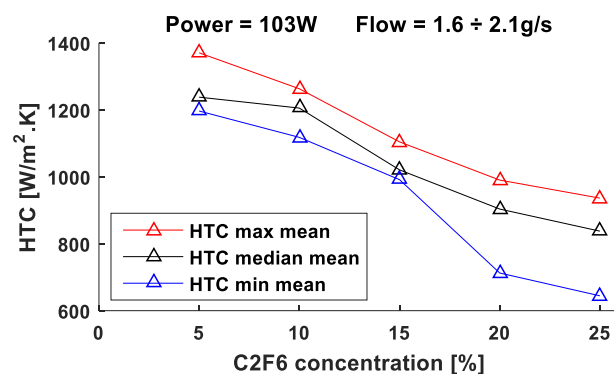


Figure 21. Heat transfer coefficient vs. mixture composition.

in the refrigerant mixture. This is probably due to the gradual change of thermomechanical properties of the refrigerant mixture. Despite the variation of flowrate, the pressure drop remains the same for all measurements, as it would have been in the case of real application.

5.10 HTC vs. vapour quality

The monitoring of saturation pressure and temperature at the stave inlet and outlet enabled us to calculate vapour quality and enthalpy, which is entering and leaving the stave. This chart is of great importance, because all models describing this phenomena employ the vapour quality as a non-dimensional parameter to reduce the complexity of the problem. This dependence has been found to be very similar for all mixtures, which were measured. Moreover, it visualizes very well the conditions inside the stave, which are also depicted in the Figure 2.

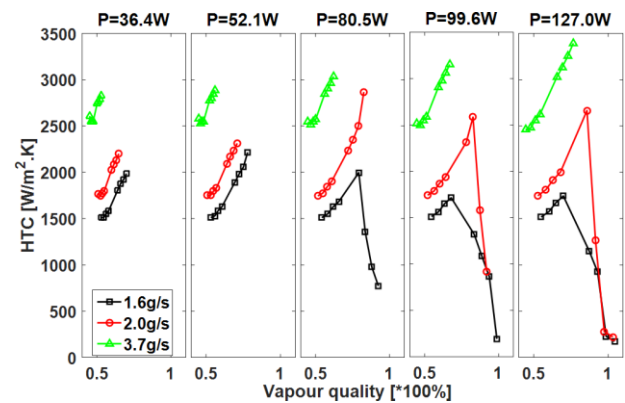


Figure 22. HTC on bottom sensors vs. vapour quality at different heat fluxes. Measurement was taken on 10% mixture.

6 Summary of results

6.1 Experimental stand

The heat transfer was investigated in smooth circular horizontal tube during the flow evaporation process. One meter long thin wall copper-nickel tube with internal diameter of 4 mm and 0.2 mm thickness was used to simulate the conditions in real stave. A direct heating was applied by means of high electric current flowing lengthwise through the tube wall. Nineteen ceramic Pt1000 2x20 mm sensors measured the temperature on the top and on the bottom of the tube. In addition, two sensors were in direct contact with the refrigerant to monitor the evaporation temperature directly at the input and output of the tube.

6.2 Investigated refrigerant mixtures

Zeotropic blends of perfluorocarbons, namely C₂F₆ and C₃F₈ were used as a working fluid in the experiments. All investigated blends exhibit complex behaviour in comparison with pure fluids or azeotropic mixtures.

Heat transfer coefficient for various heat and mass fluxes and evaporation pressures was measured and investigated for various concentrations of 5, 10, 15, 20 and 25% of C_2F_6 in C_3F_8 . The pure C_3F_8 refrigerant is yet to be measured after a necessary maintenance of the cooling circuit. Once the pure C_3F_8 is measured, it can serve as a baseline for the rest of the data.

6.3 Thermomechanical phenomena

According to the models, measurement and theory the heat transfer coefficient (HTC) depends on:

- Fluid properties and whether the fluid is pure or a zeotropic mixture
- Mass flow: the higher the mass flow the higher the turbulence and consequently the higher HTC
- Evaporation pressure
- Vapour quality
- Flow regime
- Location on the tube perimeter – the HTC may differ on the top and on the bottom of a horizontal pipe
- Other factors like surface roughness, orientation, slope, geometry of the evaporator, etc.

The heat transfer coefficient of zeotropic mixtures is lower than it would be in the case of pure components. We can clearly conclude from the presented measurements on C_3F_8 -rich mixtures, that the HTC decreases with increasing C_2F_6 concentration. Although only part of the observed HTC reduction is due to the effects related to the behaviour of zeotropic mixtures. With more C_2F_6 added to the mixture its density decreases and consequently also the mass flow through the stove is proportionally reduced, see Table 2.

6.4 Detector cooling application

It can be clearly concluded, that adding small amount of C_2F_6 in the existing C_3F_8 refrigerant effectively decreases the evaporating temperature. As a result of increasing concentration of C_2F_6 , the overall temperatures in the system gradually decrease as well. On average, every 10 % of molar fraction of C_2F_6 added to the refrigerant mixture resulted into a 4.2 °C drop of saturation temperature.

6.5 Future research

There is a challenging possibility for the future research and datamining from the gathered dataset. Some comparison of experimental data to existing analytical data, such as [9-12], and also results from dimensionless analysis is being done at present. We believe that dimensionless analysis is the option for further overall generalisation of the measurement results.

Acknowledgements

This research has been made possible from collaboration of all authors from the Department of Physics

of the Faculty of Mechanical Engineering and their participation in the ATLAS experiment at the European Organization for Nuclear Research (CERN). It has been partially supported by grant of MSMT LG 13031.

List of symbols

\dot{q}	heat flux (W/m ²)
h	heat transfer coefficient, HTC (W/m ² .K)
ΔT	temperature difference (K)

References

- [1] NOŽICKA, J. *Základy termomechaniky*. Vyd. 1. Praha: Vydavatelství CVUT, 2001, 187 s. ISBN 80-01-02409-1.
- [2] ATTREE, D. et al., 2008. The evaporative cooling system for the ATLAS inner detector. *Journal of Instrumentation*, 3(07), pp.P07003–P07003. Available at: <http://dx.doi.org/10.1088/1748-0221/3/07/p07003>.
- [3] BATES, R. et al. The cooling capabilities of C 2 F 6 / C 3 F 8 saturated fluorocarbon blends for the ATLAS silicon tracker. *J. Inst. Journal of Instrumentation*. 2015. Vol. 10, no. 03. DOI 10.1088/1748-0221/10/03/p03027.
- [4] COLLIER, John G a John R THOME. *Convective boiling and condensation*. 3rd ed. New York: Oxford University Press, 1994. ISBN 0198562829.
- [5] E.W Lemmon, .M. L. Huber, M.O. McLinden, NIST Standard Reference Database 23: Reference Fluid Thermodynamic and Transport Properties - REFPROP, Version 9.1, National Institute of Standards and Technology, Standard Reference Data Program, Gaithersburg, 2013.
- [6] VACEK, Václav, Michal VÍTEK and Martin DOUBEK, 2013. Velocity of sound in Perfluoropropane (C3F8), Perfluoroethane (C2F6) and their mixtures. *Fluid Phase Equilibria* [online]. vol. 351, pp. 53–60. Retrieved from: DOI:10.1016/j.fluid.2012.10.002
- [7] DOUBEK, M. *Thermophysical properties of fluids, experiment and simulations*. Praha: CTU Prague, 2014. Master thesis, CTU Prague, Faculty of Mechanical Engineering, Department of Fluid Dynamics and Thermodynamics.
- [8] HAUBNER, M. *Prediction of thermodynamic properties of gas mixtures using the Peng-Robinson equation of state* Praha: CTU Prague, 2014. Bachelor thesis, CTU Prague, Faculty of Mechanical Engineering, Department of Fluid Dynamics and Thermodynamics.
- [9] XU, Yu, FANG, Xiande, LI, Guohua, LI, Dingkun and YUAN, Yuliang. An experimental study of flow boiling heat transfer of R134a and evaluation of existing correlations. *International Journal of Heat and Mass Transfer*. 2016. Vol. 92, p. 1143–1157. DOI 10.1016/j.ijheatmasstransfer.2015.09.044.
- [10] FANG, Xiande, SHI, Rongrong, and ZHOU, Zhanru, 2011. Correlations of flow boiling heat transfer of R-134a in minichannels: comparative study. *Energy Science and Technology*, 1(1), pp.1-15.
- [11] ORIUNNO, M. and HEMINK, G., 2011, August. Heat Transfer Convection Measurements of Boiling CO2 in Small Horizontal Tubes at Low Temperatures. In *23rd IIR International Congress of Refrigeration, Prague, CZ*.
- [12] KANDLIKAR, S. G. A General Correlation for Saturated Two-Phase Flow Boiling Heat Transfer Inside Horizontal and Vertical Tubes. *J. Heat Transfer Journal of Heat Transfer*. 1990. Vol. 112, no. 1p. 219. DOI 10.1115/1.2910348.